Bimetallic Porous Porphyrin Polymer-Derived Non-Precious Metal Electrocatalysts for Oxygen Reduction Reactions

Sebastian Brüller,[a] Hai-Wei Liang,[a] Ulrike I. Kramm,[c] Joseph W. Krumpfer,[a] Xinliang Feng*,[b] and Klaus Müllen*[a]

Abstract: Porous conjugated networks with alternating bimetallic porphyrin sides (Fe, Co) were obtained from Suzuki polycondensation and used for the template-free preparation of metal nitrogen-doped carbons as electrocatalyst for oxygen reduction reaction (ORR). Subsequent pyrolysis of the networks reveals the key role of pre-morphology and network composition on the active sites. 57Fe-Mößbauer spectroscopy was conducted on iron catalysts (Fe; Fe/Co) to determine the coordination of Fe within the N-doped carbon matrix and the catalytic activity-enhancing shift in electron density. The bimetallic catalyst demonstrates a synergetic effect for cobalt and iron active sites, mainly through a 4-electron transfer process, achieving an onset potential of 0.87 V (versus a reversible hydrogen electrode) and half-wave potential of 0.76 V, which is only 0.08 V less than that of the state-of-the-art Pt/C catalyst. Long-term stability test reveals its superior robustness over that of the Pt/C catalyst.

1. Introduction

Electrochemical energy storage and conversion is of increasing importance to master the progressive demand for energy, urging the development of new materials applied in many technologies such as batteries, electrolysers and fuel cells. For polyelectrolyte membrane fuel cells (PEMFCs), the common catalyst for the oxygen reduction reaction (ORR) is based on Pt or Pt-alloys that suffer from high costs, scarcity and lack of stability.[1, 2] Versatile classes of materials, including molecular non-noble metal complexes, metal oxides, metal chalcogenides and metal-free heteroatom-doped carbons, have been evaluated as alternatives for Pt-based catalysts over the past several decades.[3-13] In particular, nitrogen-coordinated transition metals have received attention since Jasinski reported the electrocatalytic activity of Co-phthalocyanine in 1964.[14] However, molecular catalysts exhibit neither sufficient catalytic activity nor long-term stability due to decomplexation of the transition metal.[15] To overcome this drawback, porous carbon supports have been impregnated with nitrogen-containing transition metal complexes and subsequently converted into metal-nitrogen-doped carbon upon pyrolysis under inert atmosphere.[16-21] Thus, the activity and durability of the catalyst during the ORR process can be significantly improved.[22]

Although the detailed structure of the catalytically active sites remains elusive, it is commonly accepted that nitrogen-complexed transition metals (MN_{4-x}, M: Fe, Co, Cr, Mn) incorporated within a carbon matrix play a crucial role in ORR, particularly in acidic media.[7, 23] In addition to nitrogen-containing metal complexes such as phthalocyanines and porphyrins, which are composed of MN_4 centers, much effort has been devoted to the development of highly active ORR catalysts by simply blending individual carbon, nitrogen and metal sources or metal-chelating polymers.[21, 23-25] Although MN_4 sites can be created by thermal treatment of such precursor systems, numerous metallic nanoparticles of different size are often formed during pyrolysis.[26-28] This undesired agglomeration of metals is commonly observed for the impregnation method, in which the metal complex precursor is weakly bound or physically adsorbed on the carbon support, and leads to a decrease in the catalytic activity of these materials.[29, 30] For this reason, the optimization of the precursor composition has been intensively studied, and it has been found that a suitable amount of metal within the precursor or sulfur as an additive is necessary to limit metal nanoparticle growth.[18, 31-34] Additionally, to provide a high density of active sites as well as unhindered mass transport, the carbon support must feature a large surface area and porous structure. Therefore, hard templates, such as ordered porous silicas or metal oxides, have also been used as supports for

[a]   S. Brüller, Dr. H. W. Liang, Dr. J. W. Krumpfer, Prof. K. Müllen
       Max Planck Institute for Polymer Research
       Ackermannweg 10, 55128 Mainz, Germany
       E-mail: muellen@mpip-mainz.mpg.de
[b]   Prof. X. Feng
       Department of Chemistry and Food Chemistry, Center for
       Advancing Electronics Dresden (cfaed)
       Technical University of Dresden, Mommsenstrasse 4, 01062
       Dresden, Germany
       Email: xinliang.feng@tu-dresden.de
[c]   Prof. U. I. Kramm
       Technical University of Darmstadt
       Chair of Catalysts and Electrocatalysts
       Jovanka-Bontschits-Str. 2, 64287 Darmstadt, Germany

Supporting information for this article is given via a link at the end of the document.

ORR catalysts.[21, 35, 36] However, the removal of the costly inorganic template is difficult and increases the number of working steps. To circumvent such disadvantages, metal-organic frameworks (MOFs) have been recently reported to act as formative soft templates, which can be decomposed during pyrolysis.[37] Nevertheless, this fabrication method requires an elaborate heat treatment in a hazardous atmosphere and is associated with enormous mass loss. In the end, precursor-controlled pyrolysis of porous polymer frameworks has realized the template-free preparation of self-supporting metal-nitrogen-doped carbon materials in a one-step approach.[38] Polymer frameworks consisting of conjugated metal-porphyrins offer one route to achieving large surface areas and intrinsically porous materials with high densities of the desired MN_4 units. The immobilization of the MN_4-sites within the rigid polymer framework and its high thermal stability further alleviate the formation of metal nanoparticle agglomerates during the pyrolysis process. With respect to this finding, we recently reported the preparation of self-supported cobalt-containing nitrogen-doped carbons as ORR catalysts through pyrolysis of a porous conjugated cobalt porphyrin polymer synthesized by Yamamoto polycondensation, revealing promising electrocatalytic performance in acidic media.[39]

Numerous comparative and computational studies have indicated that iron-containing and particularly bimetallic catalysts have enhanced activity towards ORR.[40, 41] Because FeN_4-sites have a higher calculated binding energy to oxygen than CoN_4-sites, the oxygen-oxygen bond is more extended when coordinated to FeN_4-sites. Therefore, its reductive cleavage is facilitated and the evolution of hydrogen peroxide is limited. By contrast, when O_2 is adsorbed on CoN_4-sites, the probability of oxygen-oxygen bond cleavage decreases and H_2O_2 will desorb before it can be completely reduced to water. However, desorbed H_2O_2 might interact with another active site to be further reduced to water as suggested by the dependency of electrode thickness versus peroxide evolution.[42] In this manner, it is expected that bimetallic ORR catalysts with two different active sites (FeN_x and CoN_x) can favor the O_2 reduction via a direct $4e^-$ pathway or by a consecutive $2 \times 2e^-$ reaction pathway. Herein, we demonstrate a precursor-controlled pyrolysis of a bimetallic porphyrin-based conjugated microporous polymer (Fe/Co-CMP), which was synthesized by Suzuki polycondensation of iron(III) 5,10,15,20-tetrakis(4'-bromophenyl)porphine chloride ([p-Br]$_4$FeTPP, **1**) and cobalt(II) 5,10,15,20-tetrakis(4'-benzenediboronic acid bis(pinacol)

ester)porphine ([p-BOR]$_4$CoTPP, **2**), yielding a novel bimetallic (Fe/Co) catalyst with affiliated CoN_4- and FeN_4-sites. The rigidity and high thermal stability of the porphyrin network confine the formation of metal nanoparticles during the pyrolysis process, providing the retention of catalytically active MN_4-sites. ^{57}Fe-Mößbauer spectroscopy indicates a shift of electron density from neighboring CoN_4-sites to FeN_4-sites. This synergetic effect of bimetallic (Fe/Co) nitrogen-doped carbons is reflected by the higher onset potential (0.87 V) compared with the catalysts derived from monometallic porphyrin networks.

2. Experimental Section

2.1 Synthesis of (Metal-)Porphyrin Derivatives

The porphyrin monomers, 5,10,15,20-tetrakis(4'-bromophenyl)porphyrin, 5,10,15,20-tetrakis(4'-benzenediboronic acid bis(pinacol) ester) porphyrin, iron (III) 5,10,15,20-tetrakis(4'-bromophenyl)porphyrin chloride, cobalt (II) 5,10,15,20-tetrakis(4'-bromophenyl)porphyrin and cobalt(II) 5,10,15,20-tetrakis(4'-benzenediboronic acid bis(pinacol) ester) porphine, were synthesized according to the literature or with slight modifications.[43] All details regarding the synthesis and the characterization of the compounds are presented in the Supporting Information.

2.2 Synthesis of CMP

From Suzuki cross-coupling polycondensation following the procedure from the literature, metal-free, monometallic and bimetallic CMPs were obtained. Metal-free CMP: 5,10,15,20-tetrakis(4'-bromophenyl)porphyrin ([p-Br]$_4$TPP) and 5,10,15,20-tetrakis(4'-benzenediboronic acid bis(pinacol) ester) porphyrin ([p-BOR]$_4$TPP); monometallic Fe-CMP and Co-CMP: ([p-Br]$_4$FeTPP) or ([p-Br]$_4$CoTPP) and 1,4-benzenediboronic acid bis(pinacol) ester; bimetallic Fe/Co-CMP: ([p-Br]$_4$FeTPP) and ([p-BOR]$_4$CoTPP). The schematic polymer structures and their properties are displayed in Figure 1 and Figure S1.

2.3 Preparation of Pyrolyzed CMP

For the carbonization step, 200-300 mg of the CMP was put into a quartz boat, which was introduced into a ceramic oven, and pyrolyzed at various temperatures of 700, 800 and 900 °C under flowing nitrogen. First, the temperature was set to 200 °C for 2 h to remove solvents and adsorbed water from the CMP. With a

heating rate of 3 K/min the oven reached the specific temperature and held for an additional 2 h before being cooled down by natural convection. To compare structural changes – particularly the formation of nanoparticles due to the heat treatment – samples prepared at 800 °C were analyzed by SEM, TEM and EDX. For further analysis (nitrogen adsorption, XPS, electrochemical measurements, Mößbauer spectroscopy) all samples were leached by a semi concentrated (6.0 M) hydrochloric acid solution overnight. Then, the leached carbon material was filtered by vacuum filtration, washed with water and dried in air before a second pyrolysis with the same conditions as the first pyrolysis was performed. The final catalyst was used as obtained.

2.4 Characterization

Field-desorption mass spectra were measured on a VG Instrument ZAB 2-SE-FPD. Matrix-assisted laser desorption ionization time-of-flight (MALDI-TOF) experiments were conducted on a Bruker Reflex II TOF spectrometer equipped with a 337 nm nitrogen laser. Samples were analyzed from the solid state mixed within a matrix of tetracyanoquinodimethane (TCNQ). Solution UV-Vis spectra were recorded on a Perkin-Elmer Lambda 900 spectrophotometer. The spectra were correct by subtracting the background, which was measured with a cuvette filled with pure solvent. ^{1}H-NMR and ^{13}C-NMR experiments on soluble compounds were performed on the listed deuterated solvents (as internal standards) on a Bruker AMX 300, Bruker DRX 500 or Bruker DRX 700 spectrometer. Solid-state ^{13}C [^{1}H] cross polarization (CP) NMR measurements were recorded on a Bruker ASX 500 spectrometer at 75 MHz and (MAS) of 10 kHz. Fourier transformed infrared (FTIR) spectra were measured with a Nicolet 730 spectrometer equipped with an attenuated reflection (ATR) module. Thermogravimetric analysis was performed on a Toledo TGA/SDTA 851e (Mettler) with a heating rate of 5 K/min in a nitrogen atmosphere. Nitrogen sorption measurements were conducted at 77 K on a TriStar 3020 volumetric analyzer (Micromeritics). All samples were degassed at 200 °C for at least 4 h prior to every measurement. Specific surface areas were determined by standard Brunauer-Emmet-Teller (BET) method based on the relative pressure between 0.05 and 0.20. The pore size distribution (PSD) was calculated by the Barret-Joyner-Halenda (BJH) method. Scanning electron microscopy (SEM) was performed on a field emission micro analyzer (Gemini LEO 1530). Transmission electron microscopy (TEM) was carried out on a JEM-1400 (JEOL Ltd.). The sample was dispersed in ethanol by ultra-sonication and dropped onto a carbon-coated copper grid. High resolution TEM (HRTEM) and energy dispersive X-ray (EDX) measurements were conducted on a Tecnai F20 (FEI) with a beam voltage of 200 kV. X-ray photoelectron spectroscopy (XPS) was recorded on an AXIS Ultra DLD system from Kratos with an Al Kα radiation source. Mößbauer measurements were conducted at room temperature with a CMCA-550 (Wissel) equipped with a constant electronic drive system with a triangular reference waveform (Halder Electronics). The radiation source ^{57}Co/Rh was used, and the calibration of the velocity scale and the isomer shift were made with respect to α-iron.

2.5 Electrochemical Measurements

All electrochemical measurements were performed in a standard three-compartment cell using WaveDriver 20 bipotentiostat (Pine Instrument Company, USA) at room temperature. The counter electrode and reference electrode were a platinum wire and an Ag/AgCl (4 M KCl) electrode, respectively. Since all potentials in this work refer to that of reversible hydrogen electrode (RHE), a potential difference of 0.23 V – arising from the potential difference of RHE *vs.* Ag/AgCl – is taken into account. The working electrodes, a RDE composed of a glassy carbon disc (5.0 mm diameter) and a RRDE constructed of a glassy carbon disc (5.61 mm diameter) surrounded by an outer Pt-ring (6.25 mm inner-diameter and 7.92 mm outer-diameter), served as substrates for the catalyst ink. The catalyst ink was prepared by suspending 10 mg catalyst with 100 µL Nafion solution (5 wt%) and 400 µL ethanol in an ultrasonic bath. A loading of 120 µg catalyst (6 µL) was pipetted onto the glassy carbon surface of the RDE/RRDE and left to dry in air at room temperature. Before a voltammogram was recorded a reduction/oxidation cycle was performed to remove static current and weakly bond electro-active compounds. The LSVs were measured in cathodic direction using O$_2$-saturated 0.5 M H$_2$SO$_4$ as the electrolyte. The rotation speed was 1600 rpm, and the sweep rate was 5 mV/s. Since the double layer capacitance contributes to the polarization, oxygen was removed from the electrolyte by bubbling with argon for 30 min, and then a voltammogram in the O$_2$-free electrolyte was evaluated. The oxygen reduction current was determined from the difference of the voltammograms measured in O$_2$-saturated and O$_2$-free electrolyte. To determine

the peroxide generated by the ORR-catalysts, a potential of 1.4 V vs. RHE was set on the Pt-ring electrode of the RRDE.

The electron transfer number n was calculated from the following equation:

$$n = 4 \times \frac{I_D}{(I_R|N) + I_D}$$

Here, I_D and I_R are the evaluated disc and ring currents, respectively. $N = 0.37$ is the specific ring collection efficiency.

The H_2O_2 generation based on the four-electron selectivity of the catalyst is calculated from following equation:

$$H_2O_2\,(\%) = 50 \times (4 - n)$$

As state of the art material for electrochemical reactions commercial Pt on Vulcan carbon black (20 wt% from BASF) was used.

Results and Discussion

The porphyrin polymer networks were synthesized via Suzuki cross-coupling polycondensation in the presence of a catalytic amount of tetrakis(triphenylphosphine)palladium(0). Polymerization of monomers **1** and **2** produced bimetallic porphyrin polymer (Fe/Co-CMP) (Figure 1). The monometallic Co-CMP and Fe-CMP were also prepared under the same reaction conditions from 1,4-benzenediboronic acid bis(pinacol) ester with monomers **3** and **1**, respectively (for details see Experimental Section). The mono- and bimetallic CMPs were analyzed by Fourier transform infrared (FT-IR) spectroscopy and the characteristic N-Fe and N-Co vibration bands at 997 cm^{-1} and 1001 cm^{-1}, respectively, remained after the polymerization (S1a-h) indicating the stability of the formed porphyrin networks under these reaction conditions. The aryl-aryl-bond formation is further indicated by the significantly diminished intensities of the C-Br and B-O stretching band at 1072 cm^{-1} and 1348 cm^{-1}, respectively. To gain further insight into the polymerization reaction, magic angle spinning (MAS) ^{13}C-NMR spectroscopy was performed on a metal-free CMP, which was obtained from the polymerization of metal-free porphyrins 5,10,15,20-tetrakis(4'-bromophenyl)porphine and 5,10,15,20-tetrakis(4'-benzenediboronic acid bis(pinacol) ester)porphine (Figure S1i, j). With increasing reaction time, the MAS ^{13}C-NMR-spectra of the metal-free CMP displayed decreasing signal intensity for the peaks corresponding to the carbons C_{Ar}-Br (119 ppm) and C_{Ar}-B (121 ppm). Simultaneously, an increase in the peak at ~140 ppm
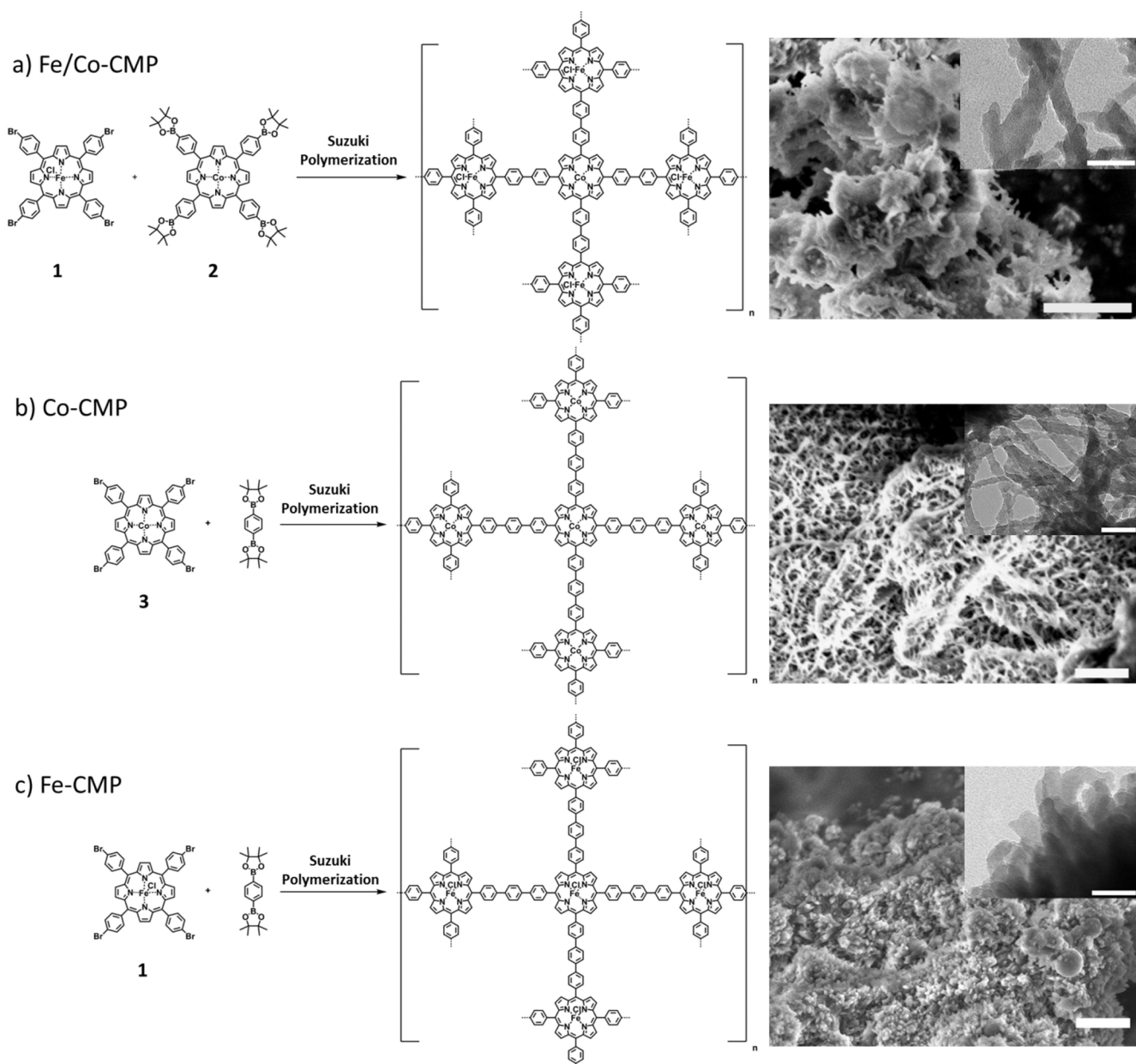
Figure 1. Schematic representation of the synthesis and structure of (a) Fe/Co-CMP, (b) Co-CMP and (c) Fe-CMP, their detailed IR-spectra revealing decrease of specific functional groups and preservation of MN_4 coordination, and their morphology imaged by SEM (scale bars 1 μm) and TEM (scale bars 0.1 μm).

– characteristic for aromatic quaternary carbons – was observed.[44] These results indicate a successful formation of CMPs with high polymerization degree.

From nitrogen adsorption measurements, the surface area was calculated by the Brunauer-Emmet-Teller method (BET) to be as high as 463, 597, 488, and 352 m^2g^{-1} for Fe/Co-CMP, Co-CMP, Fe-CMP, and metal-free CMP, respectively. These CMPs were categorized as type I isotherms, indicating that the surface area mainly consists of micropores. The absence of any hysteresis in the isotherms at low pressure indicated pore-network effects (e.g., swelling) – a characteristic property for polymers with intrinsic microporosity.[45] In the case of Fe/Co-CMP and Co-CMP, pores larger than 10 nm also contributed to the surface area (Figure S1k-n). The pyrolysis behavior of the metal-porphyrin networks was initially examined by thermal gravimetric analysis (TGA), which demonstrated a significantly elevated decomposition temperature of the rigid metal-porphyrin networks than that of the molecular porphyrins (Figure S2). Furthermore, TGA showed that Fe-CMP began to decompose at lower temperatures than the Co-containing networks, Co-CMP and Co/Fe-CMP, which both exhibited equal thermal stability and a weight loss of 26% up until 800 °C. This is likely due to the lower

stability of the iron complex and the formation of iron nanoparticles, which further catalyze the decomposition of the carbon matrix (see below). From subsequent pyrolysis of the M-CMPs in inert atmosphere at 700, 800 and 900 °C, the metal-nitrogen-doped porous carbons, which are denoted as M-CMP-700*, M-CMP-800* and M-CMP-900* (M: Fe/Co; Co; Fe), respectively, were obtained.

The morphology and nanoparticle formation in the networks after pyrolysis are shown in Figure 2. Scanning electron microscopy (SEM) analysis confirmed the retention of the microstructure in all samples after high temperature treatment, thereby demonstrating the unique thermal stability of the polymeric network. Transmission electron microscopy (TEM) revealed metal nanoparticles of 5–30 nm formed during pyrolysis are decorated on the carbon matrix. Nevertheless, the amount and diameter of the metal nanoparticles is much smaller than that of the previously reported materials based on hard and soft templates.[46, 47] A high-resolution TEM (HRTEM) investigation of Fe-CMP-800* indicated that Fe nanoparticles with diameters between 5 and 15 nm were composed of iron carbide cores encapsulated by an "onion-like" carbon shell (Figure S3). The amount and size of metal nanoparticles of Fe-CMP-800* were larger than the cobalt containing materials, which can be explained by the lower thermal stability of Fe-CMP. Furthermore, the migration of Fe nanoparticles was facilitated by the microporous, monolithic morphology of Fe-CMP-800* (Figure 2). By contrast, the morphology of Co-CMP-800* revealed a discontinuous network with a ribbon-like structure composed of fibers with diameters of 20 to 50 nm, which limits the propagation of Co nanoparticles. Similarly, the bimetallic material Fe/Co-CMP-800* exhibited fewer nanoparticles than Fe-CMP/800*, suggesting a higher retention of MN_4-sites. From HRTEM combined with energy dispersive X-ray spectroscopy (EDX), a uniform distribution of atomic cobalt and iron within a nitrogen-doped carbon matrix could be observed in Fe/Co-CMP-800* (Figures S4, S5). Based on these observations, we assume that the nucleation and diffusion of metal nanoparticles within the carbon matrix is substantially suppressed by two factors: 1) the higher thermal stability of the CoN_4-complex compared with the FeN_4-complex; 2) the microstructure composed of interconnected nanorods of cobalt-containing CMPs obtained from Suzuki polymerization. Another set of nanoparticles with diameters up to 30 nm was identified by EDX as crystalline palladium, the presence of which is attributed to the confinement of the Pd-catalyst within the polymer networks during Suzuki polymerization. These Pd nanoparticles did not reveal any significant contribution to ORR as confirmed by the ORR data of the pyrolyzed Fe- and Co-free CMPs (see below).

To expose more active sites, the metal-nanoparticles were leached out of the M-CMP-800* samples and the networks were subsequently subjected to a second heat treatment at 800 °C. These samples are denoted as Fe/Co-CMP-800, Co-CMP-800 and Fe-CMP-800, respectively. Interestingly, the surface area of Fe/Co-CMP-800 (372 m^2g^{-1}), Co-CMP-800 (334 m^2g^{-1}) and Fe-CMP-800 (373 m^2g^{-1}) independently reached similar values from the initial surface area and morphology. XPS was used to determine the chemical composition of the pyrolyzed networks. Analysis of M-CMP-800 displayed peaks for C1s, N1s, Fe 2p and/or Co 2p in all M-CMP-800 (Figure 3, S6). Additional peaks assigned to boron and oxygen arose from the decomposition products of unreacted boronic acid groups and O_2 or H_2O adsorbed from air. The overall nitrogen content of Fe-CMP-800 (2.98 %N) was lower than those of Co-CMP-800 (3.74 %N) and Fe/Co-CMP-800 (3.96 %N). This observation is in accord with the nanoparticle formation: a higher content of nanoparticles as found in Fe-CMP-800 would lead to a more pronounced destruction of active MN_4 sites.[34] Nevertheless, considering the initial content of nitrogen in the polymers (approximately 5.76 %N), a much larger relative fraction of nitrogen remained intact compared with other preparation approaches.[47] This might be due to the higher intrinsic thermal stability of the M-CMP network. The chemical nature of porphyrinic nitrogen can be transformed into several different species upon pyrolysis, such as graphitic, pyrrolic or pyridinic nitrogen. To analyze the different nitrogen-containing carbon species of the samples, the high-resolution N1s spectra was deconvoluted into its individual signals. Retention of 31 % metal-coordinated porphyrin (398.7 eV) was revealed for both Co-CMP-800 and Fe-CMP-800, whereas the ratio in Fe/Co-CMP-800 at 43 % was slightly higher. A reverse tendency was found for the ratio of graphitic nitrogen that increased in the following order: Fe/Co-CMP-800 (30 %), Co-CMP-800 (33 %) and Fe-CMP-800 (40 %). Graphitic nitrogen can enhance the conductivity of the carbon matrix, but it is not suitable for the formation of active MN_4-sites. In all samples pyrrolic and pyridinic nitrogen were formed in minor proportions. Furthermore, the metal contents of Fe-CMP-800 and Co-CMP-800 determined by XPS were 0.63 %Fe and 0.52 %Co, respectively. Fe/Co-CMP-800 revealed a total metal content of 0.86 % (0.5 %Fe, 0.36 %Co).
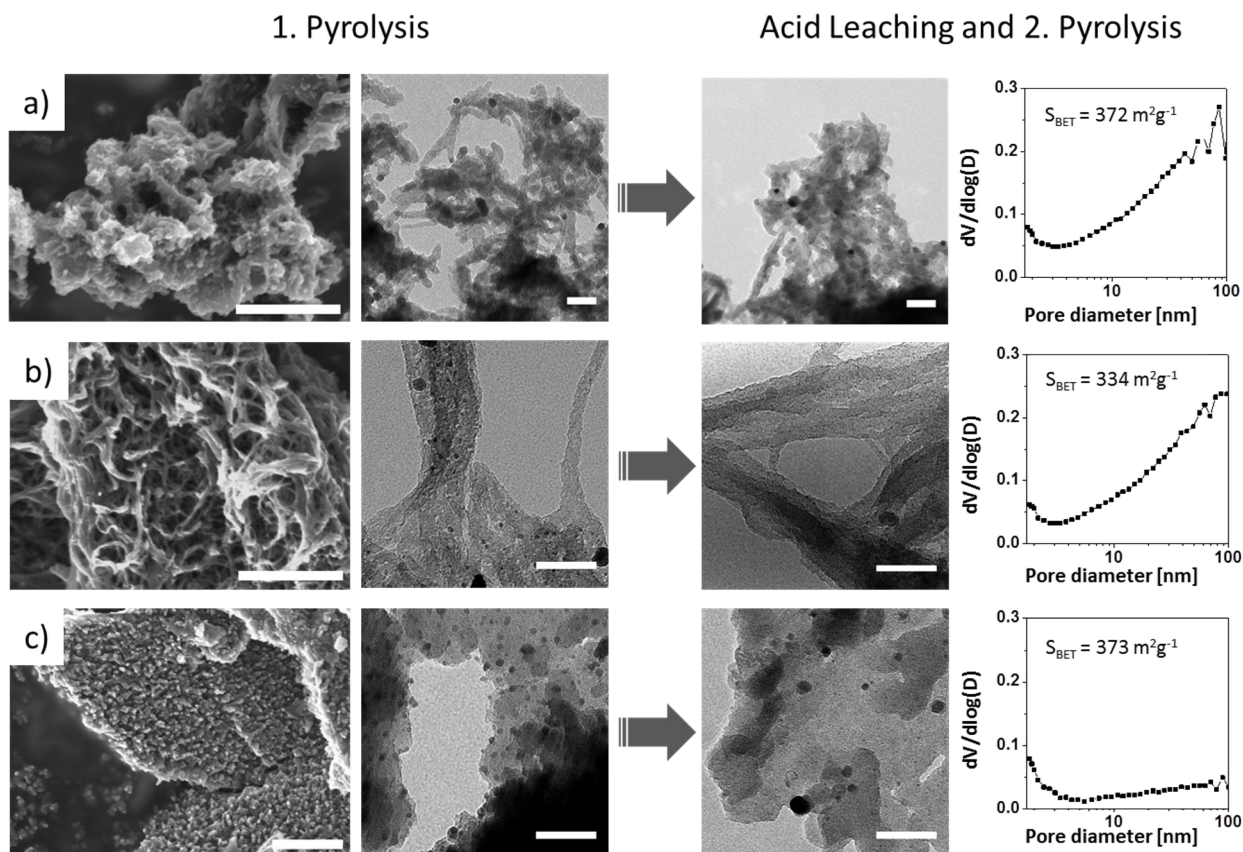
Figure 2. SEM (scale bars, 1 μm) and TEM (scale bars, 100 nm) images before and after leaching and second pyrolysis and its corresponding BET surface area and pore size distribution of (a) Fe/Co-CMP-800*, (b) Co-CMP-800* and (c) Fe-CMP-800*.

Because most of the non-coordinated metal – with the exception of encapsulated nanoparticles – was etched out, the higher metal ratio in the bimetallic catalyst Fe/Co-CMP 800 suggests the presence of more active sites.

To evaluate the nature of the active sites, the iron-containing catalysts were subjected to ^{57}Fe-Mößbauer spectroscopy studies. Structural transformations due to pyrolysis were already confirmed via high resolution nitrogen XPS. The Mößbauer spectra of both catalysts are given in Figure 4 and reveal a heterogeneous composition of the catalysts with respect to iron. Both catalysts contain three FeN$_4$-centers (D1-D3) and a minor amount of iron species without nitrogen coordination that correspond to iron nanoparticles and iron carbide. Mößbauer parameters and assignments for the iron species are summarized in Table 1. The species assignments were made by a comparison of the Mößbauer parameters of our iron sites to values reported in the literature on FeN$_4$-macrocycles and inorganic iron compounds. Major disparities between the deconvoluted spectra of both catalysts are related to the absorption areas of the different iron sites. Doublet D1 (green) corresponds to ferrous FeN$_4$ in a low-spin state (S = 0) that was

reported to be the active species towards ORR in other porphyrin-based and alternatively prepared catalysts.[26, 28, 48] The doublet D2 has Mößbauer parameters similar to those of crystalline iron phthalocyanine (FePc).[49] In its crystalline form, both the square planar nitrogen coordination as well as interactions with nitrogen atoms in the axial direction (from FePc molecules on top or below) contribute to the quadrupole splitting, which is much larger than other Fe(II)-N$_4$ sites with intermediate spin. We assume that a similarly pseudo-sixfold coordination of D2 is exclusively realized inside the material and inhibits their contribution to the catalytic activity. Doublet D3 can be assigned to the square planar Fe(II)-N$_4$ with intermediate spin.[50] In the bimetallic catalyst Fe/Co-CMP-800 doublet D1 represents the major iron species whereas the monometallic catalyst Fe-CMP-800 primarily consists of the iron species assigned to D2. Such distinct formation of iron species is reasonable in consideration of the discontinuous and the contiguous morphology of Fe/Co-CMP-800 and Fe-CMP-800, respectively. Besides morphology, the chemical structure of the precursor influences the formation and growth of iron nanoparticles which causes further destruction of active sites during heat

treatment.[29, 34] Since the lower solubility of carbon in cobalt than in iron at pyrolysis temperatures, the accumulation of nanoparticles is less pronounced for cobalt containing catalysts.[51, 52] These are important points in terms of possible optimization of the synthesis routes. Additionally, the 3d electron density at the iron center of Fe/Co-CMP-800 is more favorable for ORR catalysis, as indicated by the higher isomer shift of D1

(0.46 versus 0.42 mm s^{-1}).[26] The slightly higher absorption area of D1 and especially its higher isomer shift of Fe/Co-CMP-800 towards Fe-CMP-800 can explain the higher catalytic activity. A charge transfer from neighboring cobalt sites might be the cause of this higher isomer shift, but a more detailed investigation would be required to confirm this.
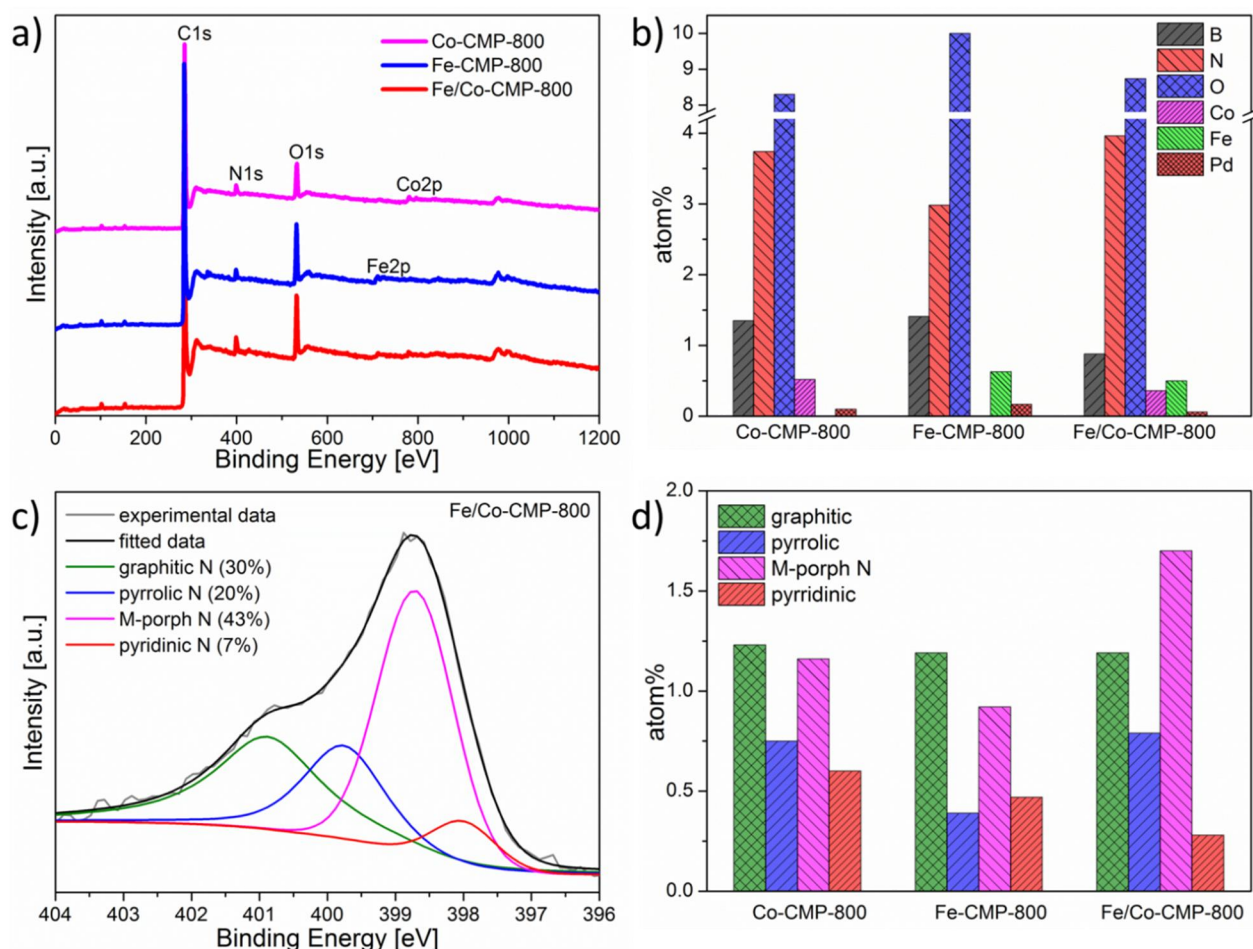

Figure 3. (a) XPS spectra recorded from 0 to 1100 eV. (b) Elemental composition of M-CMP-800 (excluding carbon). (c) High-resolution N1s XPS spectra of Fe/Co-CMP-800. (d) Content of specific nitrogen-bonding configurations in M-CMP-800.

To evaluate the ORR activity and selectivity, linear sweep voltammograms (LSV) were recorded in N$_2$- and O$_2$-saturated 0.5 M H$_2$SO$_4$ using a rotating disc electrode (RDE) with a catalyst loading of 0.6 mg cm^{-2}. First, the influence of the pyrolysis temperature on the electrocatalytic activity of Fe/Co-CMP was investigated. As displayed in Figure 5a, 800 °C was found to be the optimized pyrolysis temperature in accord with temperature-activity trends in carbon-supported porphyrin-based catalysts.[53] In Figure 5b, the polarization curves of metal-free CMP-800, Co-CMP-800, Fe-CMP, Fe/Co-CMP-800 and Pt/C are depicted. The onset-potential of the non-precious

metal-based catalysts increased in the following order: Co-CMP-800 (0.82 V), Fe-CMP-800 (0.85 V) and Fe/Co-CMP-800 (0.87 V). The metal-free catalyst CMP-800 showed poor activity, verifying the negligible contribution from the Pd-nanoparticles to ORR. These results also suggest the crucial role of FeN$_4$- and CoN$_4$-sites in nitrogen-doped carbons for the electrocatalytic reduction of oxygen in acidic media. In accordance with the intrinsic nature of the active sites, both iron-containing catalysts exhibit a similar onset potential. However, the sharp decline in the polarization curve of Fe/Co-CMP-800 suggests the presence of more exposed active sites and/or a

higher turnover frequency for the bimetallic catalyst. This behavior can be explained by the higher electron density at the iron sites, as indicated from the Mößbauer analysis. Furthermore, the half-wave potentials of Co-CMP-800 and Fe-CMP-800 were determined to be 0.72 V and 0.73 V, respectively, which are comparable values to those of other monometallic porphyrin polymer-derived catalysts.[38, 39, 54] Strikingly, the bimetallic catalyst Fe/Co-CMP-800 demonstrated a more positive half-wave potential of 0.76 V, which is only 0.08 V less than that of Pt/C (20 wt%, BASF).
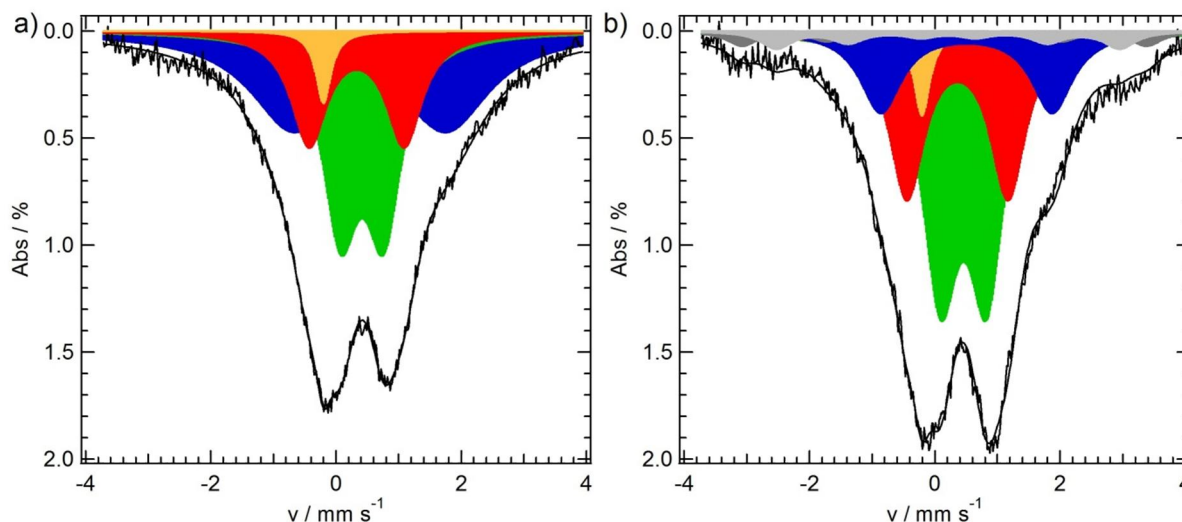

Figure 4. Mößbauer spectra of (a) Fe-CMP-800 and b) Fe/Co-CMP-800 showing ratio of assigned iron species.

Table 1. Average Mößbauer parameters of the two catalysts and assignments for the iron species.

	δ_{iso}	ΔE_Q / mm s^{-1}	fwhm	H_o / T	Fe-CMP-800 κ^2 = 0.77 A / %	Fe/Co-CMP-800 κ^2 = 1.01 A / %	Assignment
Sing	-0.21	-	0.32		2.9	3.4	Fe-nanoparticles
D1	0.44	0.71	0.7		35.1	42.7	Fe^{2+}N$_4$/C, LS[26, 47]
D2	0.53	2.60	1.2		41.0	16.1	Fe^{2+}N$_4$, MS, similar to FePc[49, 55]
D3	0.35	1.57	0.75		21.0	28.4	Fe^{2+}N$_4$/C, MS[50]
Sext a	0.15	0	0.6	20.0	-	4.3	Fe$_3$C
Sext b	0.21	0	0.6	17	-	5.1	

δ_{iso}: isomeric shift; ΔE_Q: quadrupole splitting; *fwhm*: full width at half maximum; H_o: intensity of the internal magnetic field; LS: low spin; MS: mediate spin

Aside from low overpotential, a selective reduction of oxygen to water is relevant for its application in PEMFCs. Incomplete 2e$^-$-reduction releases hydrogen peroxide, which might corrode the cell membrane and the catalyst material itself. Furthermore, the power output would strongly benefit from the complete reduction of oxygen. Therefore, the electron transfer number (ETN) of the electrocatalysts and their corresponding H$_2$O$_2$ ratios were determined by rotating ring disc electrode (RRDE) measurements (Figure 5c). From the data, the H$_2$O$_2$ evolution of Co-CMP-800 is significantly higher than that observed for the iron-containing catalysts Fe-CMP-800 and Fe/Co-CMP-800. This result indicates preferential 2e$^-$-reduction in Co-CMP-800 with respect to Fe-containing catalysts and is in accord with previous findings on selectivity in metal-nitrogen-doped catalysts.[56] Interestingly, the H$_2$O$_2$ formation for all three

catalysts increased with decreasing potential. For Co-CMP-800, it exceeded 40% at U < 0.25 V, demonstrating less selectivity for cobalt-based electrocatalysts.[57] For the iron-containing catalysts Fe-CMP-800 and Fe/Co-CMP-800, a 4e$^-$-transfer was almost exclusively observed. Particularly, in the potential range of 0.6 V to 0.8 V – that is the intended range for fuel cell applications – iron-based Fe-CMP-800 exposes a high selectivity, generating only 2.8% to 1.3% H$_2$O$_2$, respectively. In terms of selectivity, the bimetallic catalyst Fe/Co-CMP-800 (Figure 5) behaves more similarly to iron-containing Fe-CMP-800 than to Co-CMP-800. We assume that for Fe/Co-CMP-800, both active sites of FeN$_4$ and CoN$_4$ contribute to ORR. At the FeN$_4$-sites, oxygen is primarily reduced by a 4e$^-$ pathway, whereas CoN$_4$-sites tend to reduce oxygen by a 2e$^-$ pathway. In the bimetallic catalyst, H$_2$O$_2$ produced at the

CoN_4-sites can be readily reduced to water at neighboring FeN_4-sites resulting in a fast 2 x 2e$^-$ pathway. Since Fe/Co-CMP-800 is obtained from a precursor based on Suzuki polymerization, both active sites are located in close proximity, thus realizing the 2 x 2e$^-$ pathway with high efficiency. In the case of carbonized catalysts, this pathway is more likely than the proposed mechanism of nanostructured catalysts with geometrically confined active sites consisting of two MN_4 units with face-to-face arrangement of the metal centers.[58] Additionally, Fe/Co-CMP-800 demonstrates a limiting current density of 4.2 mA/cm², while Fe-CMP-800 merely reaches

3.3 mA/cm². Considering the similar specific surface areas and the equal H_2O_2 evolution of Fe/Co-CMP-800 and Fe-CMP-800, the bimetallic catalyst contains more catalytic active sites, which is in agreement with the results from the Mößbauer analysis. Furthermore, the long-term stability of Fe/Co-CMP-800 was demonstrated by performing continuous reduction/oxidation cycles (0.6 V – 1.0 V) at 50 mV/s in an oxygen-saturated electrolyte before each LSV. Our bimetallic catalyst exhibits similar stability as the commercial Pt/C catalyst, whereas other non-noble metal catalysts cannot compete with Pt/C in terms of long-term stability.[4, 59]
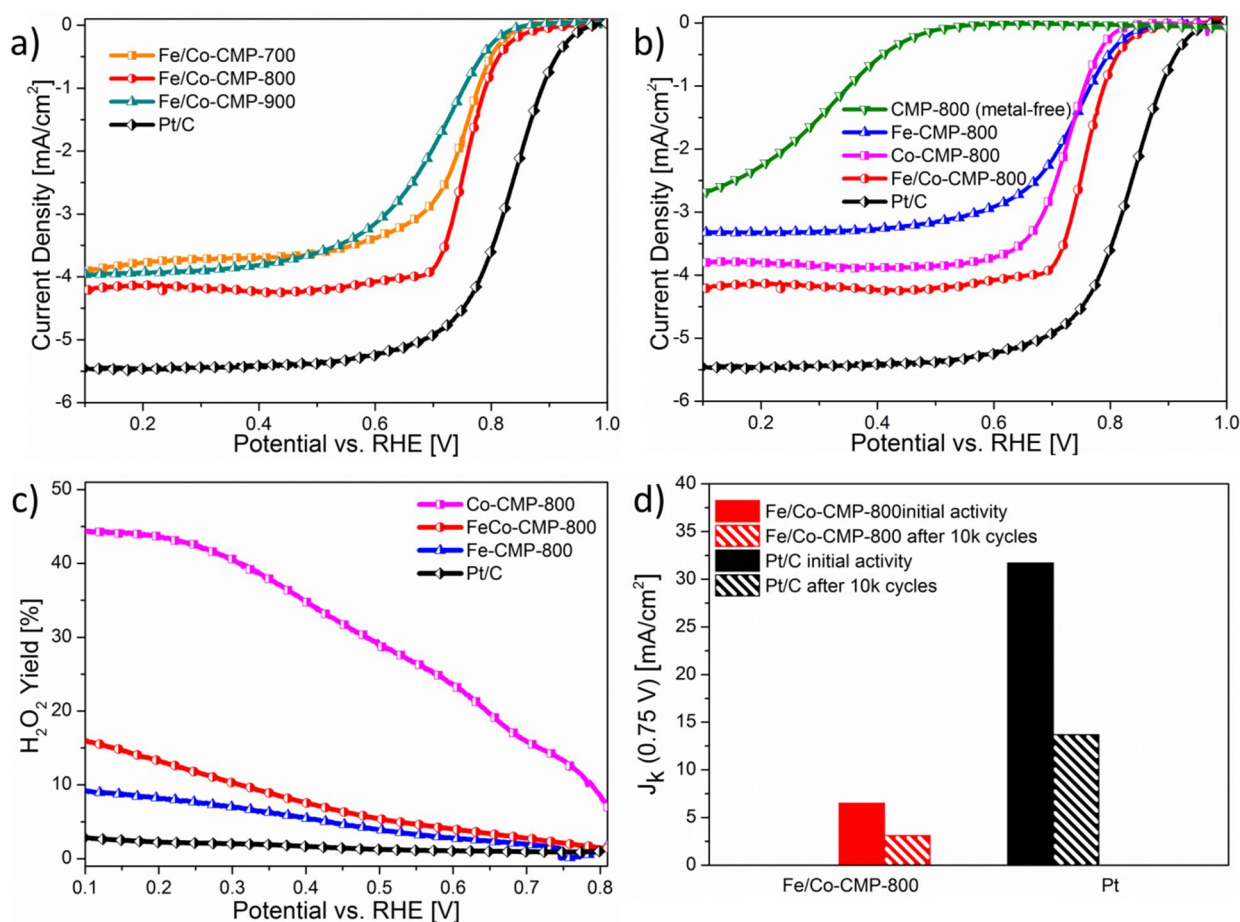

Figure 5. Electrocatalytic performance of the catalysts. (a) ORR polarization plots of Fe/Co-CMP-700, Fe/Co-CMP-800, Fe/Co-CMP-900 and Pt/C. (b) ORR polarization plots of Fe-CMP-800, Co-CMP-800, Fe/Co-CMP-800, metal-free-CMP-800 and Pt/C. (c) Electron-transfer number and corresponding H_2O_2 yield of Fe-CMP-800, Co-CMP-800, Fe/Co-CMP-800 and Pt/C. (d) Kinetic current density at 0.75 V at beginning and after 10,000 cycles. RDE and RRDE measurements were conducted in O_2-saturated 0.5 M H_2SO_4 (non-Pt catalysts) and 0.1 M $HClO_4$ (Pt/C) at 1600 rpm with a sweep rate of 5 mVs^{-1}.

Conclusions

In conclusion, we have demonstrated a template-free synthesis of Fe/Co nitrogen-doped carbon catalysts derived from the bimetallic porphyrin based conjugated polymer networks with intrinsic porosity, large surface areas, excellent thermal stability

and high densities of precisely connected MN_4 units. The bimetallic catalyst combines the physical properties of the cobalt-based catalyst (discontinuous, ribbon-like structure) with the advantages of the electrochemical properties of iron-based catalysts (high onset potential, low hydrogen peroxide evolution). Therefore, the bimetallic catalyst benefits from the two following aspects resulting in an improvement of the

electrochemical performance towards ORR: 1) due to the presence of CoN$_4$, the formation of catalytic inactive nanoparticles is diminished and the ratio of the catalytically active FeN$_4$-species is increased; 2) the poor catalytic selectivity of CoN$_4$ is compensated by the spatial proximity of CoN$_4$- and FeN$_4$-sites; and 3) a higher electron density at the FeN$_4$-sites is achieved. With this enhanced comprehension, we believe that the performance of non-precious metal-based ORR catalysts could be further improved via the rational positioning of active MN$_4$ sites in the carbon matrix, which would help develop novel electrocatalysts for various electrochemical reactions.

Acknowledgements

[1]   H. A. Gasteiger, S. S. Kocha, B. Sompalli, F. T. Wagner, *Appl. Catal., B* **2005**, *56*, 9-35.
[2]   I. E. L. Stephens, A. S. Bondarenko, U. Gronbjerg, J. Rossmeisl, I. Chorkendorff, *Energy Environ. Sci.* **2012**, *5*, 6744-6762.
[3]   Z. Yang, Z. Yao, G. Li, G. Fang, H. Nie, Z. Liu, X. Zhou, X. a. Chen, S. Huang, *ACS Nano* **2011**, *6*, 205-211.
[4]   H. R. Byon, J. Suntivich, Y. Shao-Horn, *Chem. Mater.* **2011**, *23*, 3421-3428.
[5]   F. Y. Cheng, J. A. Shen, B. Peng, Y. D. Pan, Z. L. Tao, J. Chen, *Nat. Chem.* **2011**, *3*, 79-84.
[6]   D. K. Dogutan, S. A. Stoian, R. McGuire, Jr., M. Schwalbe, T. S. Teets, D. G. Nocera, *J. Am. Chem. Soc.* **2011**, *133*, 131-140.
[7]   P. He, M. Lefevre, G. Faubert, J. P. Dodelet, *J. New Mater. Electrochem. Syst.* **1999**, *2*, 243-251.
[8]   T. Sawaguchi, T. Itabashi, T. Matsue, I. Uchida, *J. Electroanal. Chem.* **1990**, *279*, 219-230.
[9]   O. Solorzaferia, K. Ellmer, M. Giersig, N. Alonsovante, *Electrochim. Acta* **1994**, *39*, 1647-1653.
[10]   H. Behret, H. Binder, G. Sandstede, *Electrochim. Acta* **1975**, *20*, 111-117.
[11]   H. Wang, Y. Liang, Y. Li, H. Dai, *Angew. Chem. Int. Ed.* **2011**, *50*, 10969-10972.
[12]   A. Ishihara, Y. Ohgi, K. Matsuzawa, S. Mitsushima, K. Ota, *Electrochim. Acta* **2010**, *55*, 8005-8012.
[13]   F. Y. Cheng, J. Shen, W. Q. Ji, Z. L. Tao, J. Chen, *ACS App. Mater. Inter.* **2009**, *1*, 460-466.
[14]   R. Jasinski, *Nature* **1964**, *201*, 1212-1213.
[15]   K. Wiesener, *Electrochim. Acta* **1986**, *31*, 1073-1078.
[16]   T. Schilling, M. Bron, *Electrochim. Acta* **2008**, *53*, 5379-5385.
[17]   L. Birry, J. H. Zagal, J. P. Dodelet, *Electrochem. Commun.* **2010**, *12*, 628-631.
[18]   M. Ferrandon, A. J. Kropf, D. J. Myers, K. Artyushkova, U. Kramm, P. Bogdanoff, G. Wu, C. M. Johnston, P. Zelenay, *J. Phys. Chem. C* **2012**, *116*, 16001-16013.
[19]   B. Mondal, K. Sengupta, A. Rana, A. Mahammed, M. Botoshansky, S. G. Dey, Z. Gross, A. Dey, *Inorg. Chem.* **2013**, *52*, 3381-3387.
[20]   N. Larouche, R. Chenitz, M. Lefevre, E. Proietti, J. P. Dodelet, *Electrochim. Acta* **2014**, *115*, 170-182.
[21]   H. W. Liang, W. Wei, Z. S. Wu, X. L. Feng, K. Mullen, *J. Am. Chem. Soc.* **2013**, *135*, 16002-16005.
[22]   D. M. Drazic, Z. V. Ledinski, S. K. Zecevic, *J. Appl. Electrochem.* **1983**, *13*, 337-340.
[23]   S. Gupta, D. Tryk, I. Bae, W. Aldred, E. Yeager, *J. Appl. Electrochem.* **1989**, *19*, 19-27.
[24]   S. L. Gojkovic, S. Gupta, R. F. Savinell, *J. Electrochem. Soc.* **1998**, *145*, 3493-3499.
[25]   K. Lee, L. Zhang, H. Lui, R. Hui, Z. Shi, J. J. Zhang, *Electrochim. Acta* **2009**, *54*, 4704-4711.
[26]   U. I. Kramm, J. Herranz, N. Larouche, T. M. Arruda, M. Lefevre, F. Jaouen, P. Bogdanoff, S. Fiechter, I. Abs-Wurmbach, S. Mukerjee, J. P. Dodelet, *Phys. Chem. Chem. Phys.* **2012**, *14*, 11673-11688.
[27]   U. I. Kramm, I. Herrmann-Geppert, P. Bogdanoff, S. Fiechter, *J. Phys. Chem. C* **2011**, *115*, 23417-23427.
[28]   U. I. Koslowski, I. Abs-Wurmbach, S. Fiechter, P. Bogdanoff, *J. Phys. Chem. C* **2008**, *112*, 15356-15366.
[29]   C. Klinke, K. Kern, *Nanotechnology* **2007**, *18*.
[30]   C. Klinke, J. M. Bonard, K. Kern, *J. Phys. Chem. B* **2004**, *108*, 11357-11360.
[31]   U. I. Kramm, I. Herrmann, S. Fiechter, G. Zehl, I. Zizak, I. Abs-Wurmbach, J. Radnik, I. Dorbandt, P. Bogdanoff, *Proton Exch. Membr. Fuel Cells* **2009**, *25*, 659-670.
[32]   I. Herrmann, U. I. Kramm, J. Radnik, S. Fiechter, P. Bogdanoff, *J. Electrochem. Soc* **2009**, *156*, B1283-B1292.
[33]   M. Bron, S. Fiechter, M. Hilgendorff, P. Bogdanoff, *J. Appl. Electrochem.* **2002**, *32*, 211-216.
[34]   U. I. Kramm, I. Herrmann-Geppert, S. Fiechter, G. Zehl, I. Zizak, I. Dorbandt, D. Schmeisser, P. Bogdanoff, *J. Mater. Chem. A* **2014**, *2*, 2663-2670.
[35]   R. L. Liu, D. Q. Wu, X. L. Feng, K. Mullen, *Angew. Chem. Int. Ed.* **2010**, *49*, 2565-2569.
[36]   Z. S. Wu, S. B. Yang, Y. Sun, K. Parvez, X. L. Feng, K. Mullen, *J. Am. Chem. Soc.* **2012**, *134*, 9082-9085.

[37]   E. Proietti, F. Jaouen, M. Lefevre, N. Larouche, J. Tian, J. Herranz, J. P. Dodelet, *Nat. Commun.* **2011**, *2*.

[38]   S. Yuan, J. L. Shui, L. Grabstanowicz, C. Chen, S. Commet, B. Reprogle, T. Xu, L. Yu, D. J. Liu, *Angew. Chem., Int. Ed.* **2013**, *52*, 8349-8353.

[39]   Z. S. Wu, L. Chen, J. Liu, K. Parvez, H. Liang, J. Shu, H. Sachdev, R. Graf, X. Feng, K. Mullen, *Adv. Mater.* **2014**, *26*, 1450-1455.

[40]   A. Serov, M. H. Robson, M. Smolnik, P. Atanassov, *Electrochim. Acta* **2012**, *80*, 213-218.

[41]   Q. Lin, X. Bu, A. Kong, C. Mao, F. Bu, P. Feng, *Adv Mater* **2015**, *27*, 3431-3436.

[42]   A. Bonakdarpour, M. Lefevre, R. Z. Yang, F. Jaouen, T. Dahn, J. P. Dodelet, J. R. Dahn, *Electrochem. Solid-State Lett.* **2008**, *11*, B105-B108.

[43]   A. D. Adler, F. R. Longo, J. D. Finarelli, J. Goldmacher, J. Assour, L. Korsakoff, *J. Org. Chem.* **1967**, *32*, 476-476.

[44]   H. W. Spiess, in *NMR Spectroscopy of Polymers: Innovative Strategies for Complex Macromolecules, Vol. 1077*, American Chemical Society, **2011**, pp. 17-35.

[45]   K. E. Hart, J. M. Springmeier, N. B. McKeown, C. M. Colina, *Phys. Chem. Chem. Phys.* **2013**, *15*, 20161-20169.

[46]   S. L. Gojkovic, S. Gupta, R. F. Savinell, *Electrochim. Acta* **1999**, *45*, 889-897.

[47]   U. I. Kramm, M. Lefevre, N. Larouche, D. Schmeisser, J. P. Dodelet, *J. Am. Chem. Soc.* **2014**, *136*, 978-985.

[48]   J. Herranz, F. Jaouen, M. Lefevre, U. I. Kramm, E. Proietti, J. P. Dodelet, P. Bogdanoff, S. Fiechter, I. Abs-Wurmbach, P. Bertrand, T. M. Arruda, S. Mukerjee, *J. Phys. Chem. C* **2011**, *115*, 16087-16097.

[49]   R. Taube, H. Drevs, E. Fluck, P. Kuhn, K. F. Brauch, *Z. Anorg. Allg. Chem.* **1969**, *364*, 297-&.

[50]   J. T. Sage, Y. M. Xia, P. G. Debrunner, D. T. Keough, J. De Jersey, B. Zerner, *J. Am. Chem. Soc.* **1989**, *111*, 7239-7247.

[51]   C. P. Deck, K. Vecchio, *Carbon* **2006**, *44*, 267-275.

[52]   L. Dignardbailey, M. L. Trudeau, A. Joly, R. Schulz, G. Lalande, D. Guay, J. P. Dodelet, *J. Mater. Res.* **1994**, *9*, 3203-3209.

[53]   U. I. Kramm, I. Abs-Wurmbach, I. Herrmann-Geppert, J. Radnik, S. Fiechter, P. Bogdanoff, *J. Electrochem. Soc.* **2011**, *158*, B69-B78.

[54]   Z. Xiang, Y. Xue, D. Cao, L. Huang, J. F. Chen, L. Dai, *Angew. Chem. Int. Ed.* **2014**, *53*, 2433-2437.

[55]   C. A. Melendres, *J. Phys. Chem.* **1980**, *84*, 1936-1939.

[56]   G. Wu, K. L. More, C. M. Johnston, P. Zelenay, *Science* **2011**, *332*, 443-447.

[57]   S. Marcotte, D. Villers, N. Guillet, L. Roué, J. P. Dodelet, *Electrochim. Acta* **2004**, *50*, 179-188.

[58]   J. Y. Cheon, T. Kim, Y. Choi, H. Y. Jeong, M. G. Kim, Y. J. Sa, J. Kim, Z. Lee, T. H. Yang, K. Kwon, O. Terasaki, G. G. Park, R. R. Adzic, S. H. Joo, *Sci. Rep.* **2013**, *3*, 2715.

[59]   F. Hasche, M. Oezaslan, P. Strasser, *Phys. Chem. Chem. Phys.* **2010**, *12*, 15251-15258.

FULL PAPER
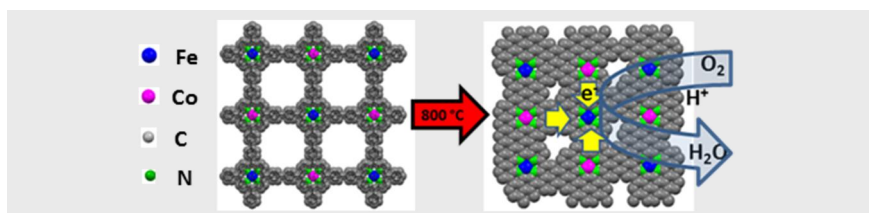
Bimetallic (Fe/Co) nitrogen-doped carbons as electrocatalysts for oxygen reduction reaction are prepared from conjugated, microporous metal-porphyrin networks composed of alternating metal complexes with CoN_4- and FeN_4-centers. In acidic media, the bimetallic catalyst demonstrates a synergetic effect at cobalt and iron active sites for reducing oxygen efficiently with a half-wave potential of 0.76 V, which is only 0.08 V less than that of the Pt/C.

Sebastian Brüller, Hai-Wei Liang, Ulrike I. Kramm, Joseph W. Krumpfer, Xinliang Feng[*], and Klaus Müllen[*]

Bimetallic porous porphyrin polymer-derived non-precious metal electrocatalysts for oxygen reduction reactions